Experimental Study of the Energy and Exergy performance for a Pressurized Volumetric Solar Receiver

Jianqin Zhu[a], Kai Wang[b,*], Zhaowu Jiang[b], Hongwei Wu[c,**],

Dunjin Wang[b], Feng Lin[b], Yongliang Li[d]

[a] National Key Lab. of Science and Technology on Aero-Engines,

School of Energy and Power Engineering, Beihang University, Beijing 100191, China

[b] Institute of Engineering Thermophysics, Chinese Academy of Sciences,
Beijing, 100190, China.

[c] Department of Mechanical and Construction Engineering, Faculty of Engineering and Environment,
Northumbria University, Newcastle upon Tyne, NE1 8ST, United Kingdom

[d] School of Chemical Engineering, University of Birmingham,
Edgbaston, Birmingham B15 2TT United Kingdom

[*]Corresponding author.   Email: wang_kai@iet.cn   Tel. +86(10)82543147 Fax. +86(10)82613328

[**]Corresponding author.   Email: hongwei.wu@northumbria.ac.uk   Tel. +44(0)1913495365

Abstract

This article presents an experimental investigation of the heat transfer characteristics as well as energy and exergy performance for a pressurised volumetric solar receiver under variable mass flow rate conditions. During a two hour period of continuous operation in the morning, the solar irradiance is relatively stable and maintained at approximately 600 W/m^2, which is beneficial for analyzing the energy and exergy performance of the solar receiver. Experimental results show that the mass flow rate fluctuation has slight effect on the solar receiver outlet temperature. Whereas the mass flow rate plays an important role in the solar receiver power, energy efficiency and exergy efficiency. The efficiency of the solar receiver is normally above 55% with the highest efficiency of 87%, and at steady state, the efficiency is maintained at around 60%. A very low value of the heat loss factor (0.014 kW/K) could be achieved during the current steady state operating conditions. The highest exergy efficiency is approximately 36%. In addition, as the temperature

31 difference increases, the impact of the exergy factor increases. The highest exergy

32 factor is 0.41 during the entire test.

33 **Keywords:** solar receiver; exergy; energy efficiency; heat transfer; radiation.

34

Nomenclature			
A_{ap}	effective aperture area of dish [m^2]	Ex_s	rate of solar exergy delivery [kw]
A_p	project area [m^2]	G	direct solar radiation [w/m^2]
c_{av}	average specific heat capacity [J/kg·K]	$\dot{m}$	mass flow rate [kg/s]
D_f	focus point diameter [m]	n_d	parabolic dish combined optical efficiency [-]
E_D	concentrated solar radiation power [kw]	r_c	concentration ratio
E_L	heat loss [kw]	T_{in}	inlet temperature of the air [K]
E_R	receiver power [kw]	T_{out}	outlet temperature of the air[K]
E_S	solar radiation power on the dish [kw]	T_{ave}	average temperature of the air[K]
Ex_D	rate of dish exergy concentrated [kw]	U_L	heat loss coefficient [kw/m^{2}K]
Ex_f	exergy factor [-]	$\eta_{th.R}$	energy efficiency of the receiver [-]
Ex_R	receiver exergy [kw]	$\eta_{ex.R}$	exergy efficiency of the receiver [-]

35

1. Introduction

37   With rapidly increasing energy prices and globalization, process industries seek

38 opportunities to reduce production costs and improve energy efficiency. Among the

39 energy-efficient technologies, Concentrated Solar Power (CSP) system is considered

40 as one of the most attractive ways to solve the energy crisis in the future [1,2]. Many

41 developed countries like the United State and the European Commission have been

42 devoted to the solarised Brayton micro-turbines system over the past decades [3-5].

43   Compared to the traditional gas turbine, solarised Brayton turbines use solar

44 receiver to replace the combustion chamber in the traditional gas turbine [6]. The

45 solar concentration part which is used to provide high temperature air is very crucial

46 for the entire solar power system. The system efficiency and the cost of the power

47 generation are highly depended on the solar concentration conversion efficiency from

48 solar radiation to thermal fluid. Thus, the solar concentration part has to be well

49 designed in order to achieve high efficiency and low pressure loss. Many studies have

50 been devoted to the design and performance of the receiver. Neber and Lee [7]

51 designed a high temperature cavity receiver using silicon carbide. Then a scaled test

52 section was placed at the focal point of a parabolic dish collector and reached a

53 maximum temperature of 1248 K. Fernandez et al. [8] presented a multidisciplinary

54 design optimization of a 5 MW Small Particle Heat Exchange Receiver (SPHER) for

55 a central receiver solar plants. The new developed solar receiver aims to heat air to

56 temperatures in excess of 1300 K and use this high-temperature energy to drive a

57 Brayton cycle or a combined Brayton/Rankine cycle. It was found that the receiver

58 efficiency can be increased by 6% with respect to the previous baseline design from

59 the same author [9]. Buck et al. [10] introduced a receiver module consisting of a

60 secondary concentrator and a volumetric receiver unit which was closed with a domed

61 quartz window to transmit the concentrated solar radiation. Hischier et al. [11, 12]

62   proposed a novel design of a high-temperature pressurized solar air receiver for power

63   generation via combined Brayton-Rankine cycles. It consists of an annular reticulate

64   porous ceramic bounded by two concentric cylinders. The heat transfer mechanism

65   was analyzed by the finite volume technique and by using the Rosseland diffusion, P1,

66   and Monte-Carlo radiation method. It was found that, for a solar concentration ratio of

67   3000 suns, the outlet air temperature can reach 1000 °C at 10 bars, yielding a thermal

68   efficiency of 78%.

69   It is recognized that the flow and heat transfer processes in the solar receiver are

70   very complicated. Over the past years, many studies have been devoted to the

71   optimization of the design using theoretical and numerical method. Cui et al. [13]

72   developed a three-dimensional optical model and simulated the solar transmission

73   process for a pressurized volumetric receiver using the Monte Carlo Ray Tracing

74   (MCRT) method. Wang et al. [14] developed a three-dimensional model of parabolic

75   dish-receiver system with argon gas as the working fluid to simulate the thermal

76   performance of a dish-type concentrated solar energy system. Lu et al. [15] proposed

77   heat and mass transfer models of the solar heat receiver, and associated heat

78   absorption and exergetic performance were further investigated by considering the

79   heat loss outside the receiver and fluid viscous dissipation inside the receiver. Song et

80   al. [16] analyzed the effect of the solar incidence angle in order to accurately simulate

81   the heat flux distribution around the absorber tube outer surface. Le Roux et al. [17]

82   investigated the effect of wind, receiver inclination, rim angle, atmospheric

83   temperature and pressure, recuperator height, solar irradiance and concentration ratio

84   on the optimum geometries and performance. Lu et al. [18] theoretically investigated

85   the nonuniform heat transfer model and performance of parabolic trough solar

86   receiver and the results showed that the heat loss of solar receiver from the

87   nonuniform model is a slight higher than that from the uniform model.

88   On the other hand, many numerical research works are also conducted to simulate

89   the detail heat transfer process. Flesch et al. [19] numerically analyzed the impact of

90   head-on and side-on wind on large cavity receivers with inclination angles ranges

91   from $0°$ (horizontal cavity) to $90°$ (vertical cavity) and compared with the data

92   published in the open literature. Wei et al. [20] presented an original CFD-based

93   evolutionary algorithm to determine the optimal fluid distribution in a tubular solar

94   receiver for the minimization of its peak temperature. Tu et al. [21] proposed a

95   modified combined method to simulate the thermal performance of a saturated

96   water/steam solar cavity receiver. Capeillere et al. [22] numerically studied the

97   thermomechanical behavior of a plate solar receiver with asymmetric heating. The

98   numerical results showed that the choice of the shape and levels of the solar irradiance

99   map is crucial. The distribution of the most relevant incident solar flux and the

100   geometry compromise were determined. Wang et al. [23] conducted a numerical

101   study focusing on the thermal performance of porous medium receiver with quartz

102   window. Their results indicated that the pressure distribution and temperature

103   distribution for the condition of fluid inlet located at the side wall was different from

104   that for the condition of fluid inlet located at the front surface.

105   Exergy analysis has been applied in various power studies [24-26].

106   Thermodynamic analyses and optimization of a recompression N_2O Brayton power

107   cycle have been performed [27]. The performance of a regenerative Brayton heat

108   engine has been studied by focusing on the minimization of irreversibility [28]. In the

109   authors' earlier studies [29, 30], a coiled tube solar receiver has been designed and

110   tested in the real solar radiation condition. But due to the limitation of the tube

111   material, the coiled tube solar receiver can not achieve very high temperature. Thus, a

112   pressurized volumetric solar receiver using metal foam as thermal absorbing core is

113   designed in this work. It appears from the previous investigation that the key point for

114   the solarised Brayton micro-turbines is to develop solar receivers which have terrific

115   performance on the pressure loss and heat transfer. To the best of the authors'

116   knowledge, there is a lack of available experimental data under real concentrate solar

117   and variable mass flow conditions especially for the cases of extremely high heat flux

118   and high temperature. To this end, the present research is aimed to experimentally

119   analyze both the efficiency and heat loss of a pressurized volumetric solar receiver

120   under real solar radiation and variable mass flow conditions in more detail.

121

122   **2. Experimental apparatus and method**

123   *2.1. Experimental apparatus*

124   The experimental study was conducted at a location with the geographical

125   position of 30°36' latitude and 120°22' longitude, Hangzhou, China. The whole

126   system, shown schematically in Fig. 1, mainly consists of three components: dish,

127   compressor and receiver. The dish used for the experimental tests of the developed

128   solar heat receiver was listed in Fig. 2. All 40 trapezoidal, pre-bent mirrors are resin

129   molded and laminated. The reflective surface is applied as an adhesive foil. At the

130   bottom of the dish a cut out is made for the tower. The main dish parameters utilized

131   in the current study are illustrated in Table 1, which is provided by the dish reflector

132   manufacturer. To make sure that the light reflected by the mirror focus on the aperture

133   of the receiver, each mirror was adjusted carefully.

134   The dish is controlled by a solar tracker which is embedded in the inner program to

135   make the dish face the Sun automatically. The inner program could accurately

136   calculate the attitude angle in terms of the dish location of the earth and the local time.

137   As illustrated in Fig. 1, the attitude angel is formed between the boom line and

138   horizon line. A stepping motor can be well controlled to change the dish attitude angle

139   slowly. When the dish is in operation during the morning, the attitude angle is lower

140   than $40°$ for the sun just rising over the horizontal line. Whereas the dish is operated

141   in the noon, the attitude angle is approximately $80°$. It should be recognized that the

142   initial setting for the location and accurate time is very crucial during the test. An

143   uninterruptible power supply (UPS) system is also adopted to assist the dish off the

144   solar direction in some emergency to further protect the receiver. During the

145   experiments, a 20 kw piston compressor driven by the electricity is used to compress

146   the air. The pressurized air is compressed at environmental temperature and pressure.

147   After the filter, the air is pressurized into the air tank with the pressure of 0.8 Mpa to

148   guarantee the enough air flow during the experiment process. After that the

149   pressurized air is supplied into the receiver. Two valves are installed at the receiver

150   inlet and outlet to ensure the receiver works under designed pressure about 0.4 Mpa.

151   Because the light incident surface of the receiver is made of quartz glass, too high

152   pressure could damage the receiver. Hence, by adjusting this valve, the pressure of the

153   whole system as well as the portion of the receiver can be well controlled. The output

154   mass flow rate is variable. Thermocouple and pressure sensor are placed at the inlet

155   and outlet of the pipe respectively to obtain the receiver efficiency and heat loss. The

156   receiver itself is mounted onto the cantilever arm. In the current study, the heat flux of

157   the focus power could achieve 1000 kW/m^2 for the dish concentrator has the

158   concentrate ratio of 1750. It can be expected that, except for the receiver and

159   protecting panel, other components of the system would be burned in a short time. To

160   protect other part of the receiver from misaligned radiation an additional protecting

161   panel is mounted circumferentially to the receiver. As shown in Fig. 3, the protecting

162   panel is made of Calcium silicate board with 10 mm in thickness. The diameter of the

163   aperture in the protecting panel is 250 mm. Four K-type thermocouples with an

164   accuracy of 0.5 °C are fixed on the back to monitor the temperature of the protecting

165   panel. When the temperature is over 850 ℃, it means that the concentrate solar spot is

166   not located into the aperture. As a result, the inner program has to be reset to adjust

167   the attitude angle in order to prevent fatal damage.

168   *2.2. Solar receiver model*

169   For the current experimental evaluation, as shown in Fig. 4, the solar receiver is

170   designed as a type of pressurized volumetric solar receiver. Fig. 4(a) shows the 3D

171   view of the model and Fig. 4(b) presents the cross sectional view of the receiver. The

172   advantage of the pressurized volumetric solar receiver is high outlet air temperature

173   and high thermal efficiency. It should be stressed here that the key point for the design

174   of the pressurized volumetric solar receiver is the cooling of the light incident glass

175   and the equally distributed mass flow in the heat absorbing core. The light incident

176   glass is made of quartz glass which can endure a temperature up to $1500\,C^{\circ}$. But the

177   concentrated solar focuses on the quartz glass directly, the glass cooling using the

178   inlet air could extend the life span of the receiver and make the receiver working

179   process more secure. For this reason, a big inlet tube is used with the diameter of 50

180   mm. The pressured air is injected into the inlet tube, and then, it is divided into three

181   small tubes with the diameter of 20 mm. The three small tubes that circumferentially

182   uniformly distributed are welded at the end of the pressure cavity which forms the

183   main part of the solar receiver. The air flow along the edge of the cavity and inject on

184   the quartz glass forming the cooling of the light incident glass. The diameter and the

185   height of the main part of the receiver are 400 mm and 360 mm, respectively. The

186   concentrate solar radiation (CSR) passes through the quartz glass and heat the

187   absorbing core. As shown in Fig. 5, the material of the absorbing core is Nickel foam

188   which could endure the temperature up to 1453 ℃. To increase the absorbing ability,

189   65mm Nickel foam with the PPI (Pores per Inch) value of 75 is selected. PPI which is

190   a common parameter is usually used in industry to indicate the pore diameter of the

191   metal foam. The 75 PPM value means that the pore diameter is about 0.34 mm. One

192   can imagine that the small pore diameter would enhance the heat transfer coefficient

193   and heat transfer area easily. At last, to minimize the heat loss, the receiver is

194   surrounded by Aluminum silicate whose heat conductivity coefficient is

195    $0.06 \, \text{W/m}^2 \, \text{K}^{-1}$.

196   *2.3. Energy and exergy analysis*

197   Experimental energy and exergy parameters to characterize the thermal

198   performance of the receiver are presented in this section.

199   *2.3.1. Energy analysis* [31, 32]

200   The energy that the whole system receives comes from the solar radiation. The

201   solar radiation power on the parabolic dish reflector can be expressed as:

202    $E_S = A_{ap} G$

203   (1)

204   where E_S is the solar radiation power on the dish, A_{ap} is the effective aperture

205   area of the parabolic dish, and G is the direct solar irradiation from the Sun to the dish.

206   G is measured with a normal incidence pyrheliometer (NIP) Hukseflux DR01

207   attached to the solar tracker.

208   The solar radiation is concentrated and delivered to the receiver by the parabolic

209   dish. The concentrated solar radiation power (E_D) can be expressed as:

210     $$E_D = n_d E_S = n_d A_{ap} G \qquad (2)$$

211   where E_D is the concentrated solar radiation power from parabolic dish to the

212   receiver, n_d is the parabolic dish combined with optical efficiency described in

213   Table 1.

214   The concentrated solar radiation on the receiver is absorbed by the heat-transfer

215   fluid flowing in the pressurized cavity of the receiver. The energy rate that air absorbs

216   or receives power is given by:

217     $$E_R = \dot{m} c_{av}(T_{out} - T_{in}) \qquad (3)$$

218   where $\dot{m}$ is the mass flow rate of the air, c_{av} is the average specific heat

219   capacity of the air which is a function of the average air inlet temperature (T_{in}) and air

220   outlet temperature (T_{out}). The average temperature of the receiver (T_{ave}) can be

221   defined by:

222     $$T_{ave} = (T_{in} + T_{out})/2 \qquad (4)$$

223   Thus, the relation between the average specific heat capacity of the air and the

224   average temperature can be obtained as:

225     $$c_{av} = 0.9956 + 0.000093 T_{ave} \qquad (5)$$

226   Based on the energy conservation, the receiver power is the difference between

227   the concentrated solar radiation power and the overall heat losses are relative low. The

228   receiver power can also be described as

229     $E_R = E_D - E_L$ (6)

230   where E_L is the rate of the heat loss from the receiver to the surroundings,

231   which contains the convective heat losses, conductive heat losses and radioactive heat

232   losses. E_L can be expressed as

233     $E_L = U_L A_R (T_{ave} - T_{amb})$ (7)

234   where U_L is the total heat loss coefficient determined, A_R is the effective

235   receiver area, and T_{amb} is the ambient temperature. The product $U_L A_R$ is referred as

236   the heat loss factor given by

237     $U_L' = U_L A_R$

238   (8)

239   Therefore, combination of Eqs (2), (3), (6) and (7) can yield

240     $\dot{m} c_{av} (T_{out} - T_{in}) = n_d A_{ap} G - U_L' (T_{ave} - T_{amb})$

241   (9)

242   The thermal energy efficiency of the receiver is defined as the ratio of the

243   receiver power to the concentrated solar radiation power from the parabolic dish to

244   the receiver which is expressed as:

245     $\eta_{th.R} = \dfrac{E_R}{E_D} = \dfrac{\dot{m} c_{av} (T_{out} - T_{in})}{n_d A_{ap} G}$

246   (10)

247   By dividing $A_{ap} G$ on both side of Eq. (9) and combine with Eq. (10) leads to

248     $\eta_{th.R} n_d = n_d - \dfrac{U_L' (T_{ave} - T_{amb})}{A_{ap} G}$ (11)

249   *2.3.2 Exergy analysis* [31, 32]

250   The exergy rate of the receiver or the quality of the energy delivered to the

251   circulating fluid with reference to the surroundings can be expressed as

252     $Ex_R = E_R - \dot{m}c_{av}T_{amb}\ln\left(\frac{T_{out}}{T_{in}}\right)$ (12)

253   Substituting Eq. (3) into Eq. (12) yields

254     $Ex_R = \dot{m}c_{av}\left[(T_{out} - T_{in}) - T_{amb}\ln\left(\frac{T_{out}}{T_{in}}\right)\right]$ (13)

255   The rate of the solar exergy delivery by the Sun to the dish and then to the

256   concentrator is given by the Petela expression [33] and is expressed as

257     $Ex_s = GA_{ap}\left[1 + \frac{1}{3}\left(\frac{T_{amb}}{T_s}\right)^4 - \frac{4T_{amb}}{3T_s}\right]$ (14)

258   where T_s is the surface temperature of the Sun which is approximately 5762 K.

259   So the concentrated solar radiation exergy (Ex_D) can be expressed as:

260     $Ex_D = n_d GA_{ap}\left[1 + \frac{1}{3}\left(\frac{T_{amb}}{T_s}\right)^4 - \frac{4T_{amb}}{3T_s}\right]$

261   (15)

262   The exergy efficiency is defined as the ratio of the receiver exergy rate to the rate

263   of the concentrated solar radiation exergy and can be determined as follows:

264     $\eta_{ex.R} = \frac{Ex_R}{Ex_D} = \frac{\dot{m}c_{av}\left[(T_{out}-T_{in})-T_{amb}\ln\left(\frac{T_{out}}{T_{in}}\right)\right]}{n_d GA_{ap}\left[1+\frac{1}{3}\left(\frac{T_{amb}}{T_s}\right)^4 - \frac{4T_{amb}}{3T_s}\right]}$ (16)

265   The exergy factor is defined as the ratio of the receiver exergy rate to the

266   receiver energy rate and can be represented by equation:

267     $Ex_f = \frac{Ex_R}{E_R} = \frac{\dot{m}c_{av}\left[(T_{out}-T_{in})-T_{amb}\ln\left(\frac{T_{out}}{T_{in}}\right)\right]}{\dot{m}c_{av}(T_{out}-T_{in})}$ (17)

268   **3. Uncertainty analysis**

269   The uncertainties of the measurement in the experiment are dependent on the

270   experimental conditions and the measurement instruments. An uncertainty analysis is

271   performed on the receiver power E_R and the receiver exergy Ex_R, which are the

272   most important derived quantities from the measurements of using the propagation of

273   error method described by Moffat [34]. The uncertainty of the receiver power could

274   be calculated by the following equation:

275    $$\delta E_R = \sqrt{\left(\frac{\delta E_R}{\delta \dot{m}}\right)^2 (\delta \dot{m})^2 + \left(\frac{\delta E_R}{\delta T_{out}}\right)^2 (\delta T_{out})^2 + \left(\frac{\delta E_R}{\delta T_{in}}\right)^2 (\delta T_{in})^2} \qquad (17)$$

276   While the uncertainty of the receiver exergy rate is given by

277    $$\delta Ex_R = \sqrt{\begin{array}{c} \left(\frac{\delta Ex_R}{\delta \dot{m}}\right)^2 (\delta \dot{m})^2 + \left(\frac{\delta Ex_R}{\delta T_{out}}\right)^2 (\delta T_{out})^2 \\ + \left(\frac{\delta Ex_R}{\delta T_{in}}\right)^2 (\delta T_{in})^2 + \left(\frac{\delta Ex_R}{\delta T_{amb}}\right)^2 (\delta T_{amb})^2 \end{array}} \qquad (18)$$

278   In the current study, the main uncertainty parameters are the mass flow rate ($\dot{m}$),

279   the inlet temperature (T_{in}), and the outlet temperature (T_{out}). The relative uncertainty

280   of the mass flow rate is given by the float flowmeter with the value of 2%. Therefore,

281    $\delta \dot{m} = 2\% \times \dot{m} = \pm 0.001 \; kg/s$. The uncertainty of the temperature is given by the

282   K-type thermocouple with the value of $\delta T_{out} = \delta T_{in} = \pm 0.5 \; K$.

283   The maximum experimental values for the receiver power and exergy rate are

284   around 18.5 kW and 7.28 kW, respectively. The uncertainty of the receiver power is

285   0.372 kW, and the uncertainty of the receiver exergy rate is 0.147 kW. Overall, the

286   overall uncertainty of the receiver power and exergy rate are 2.01% and 2.02%,

287   respectively.

288   **4. Results and discussion**

289   Fig. 6 shows the variation of the solar irradiance (G) during a test period from

290   10:00 am to 13:30 pm. The experimental data were collected on November 6th, 2015,

291 which is a local autumn season in Hangzhou, China. According to Fig. 6, it is shown

292 that the solar irradiance fluctuates at around 600 W/m^2 all the time. And the solar

293 irradiance data increases slowly with time except two fast drops observed in the

294 afternoon for about 15 mins. The reason could be due to the fact that two short period

295 of passing cloud occurred. From this figure, it can be seen clearly that the solar

296 irradiance is almost stable and maintained at around 600 W/m^2 from 10:00 am to

297 12:00 pm. It is obviously that the stable solar irradiation condition is beneficial for

298 analyzing the energy and exergy performance of the solar receiver. For this purpose, a

299 test period of continuous 2 h from 10:00 am to 12:00 pm is selected. Dynamic

300 acquisition system is used to record the parameters automatically during the test. The

301 ambient temperature is maintained at around 25 ℃ during the experiment process.

302 Fig. 7 shows the variation of the inlet pressure, outlet pressure and mass flow rate. For

303 the design pressure of the solar receiver is 0.4 Mpa, the experiment should be

304 conducted at the same pressure. Since the heating from the concentrate solar

305 irradiation could lead to the rising of the internal pressure, the inlet valve is adjusted

306 during the experimental process to ensure the solar receiver working safety. Therefore,

307 the mass flow rate fluctuates all the time. The average value of the mass flow rate is

308 about 0.036 kg/s. In the current study, the main purpose is to test the energy and

309 exergy performance of the solar receiver under the fluctuant mass flow rate condition.

310 Fig. 8 presents the time series of air temperatures at the inlet and outlet of the

311 receiver. The inlet temperature maintains nearly constant about 42 ℃. The outlet

312   temperature rises very quickly at the starting stage, and achieves the highest

313   temperature of 480 ℃ at the end of the experiment process. From 10:00 am to 10:30

314   am, it takes about half an hour to rise the solar receiver outlet temperature from 42℃

315   to 430℃. After 10:30 am, the outlet temperature increases very slowly with the time.

316   The first half an hour is used for preheating. It is due to the fact that the receiver tubes

317   are surrounded by the insulation materials with high specific heat capability (*Cp*). It is

318   noteworthy that the rising speed of the receiver efficiency is very high within the first

319   30 mins. This phenomenon is very important and should be stressed here since the

320   sunshine is limited in the day time, quick start up can make the overall solar power

321   generation system to generate more electricity. Therefore, the cost of the power

322   generation will be lower and the investment recovery period could be shorter. There is

323   also another interesting phenomenon that the mass flow rate fluctuation has little

324   effect on the solar receiver outlet temperature. It may be due to the reason that the

325   porous metal is used as the heat absorbing core. The pore size is very small with the

326   value about 0.34 mm. This small size pore could increase the heat transfer coefficient

327   and area obviously. The heat transfer between the porous metal and the air is strong

328   enough that the air outlet temperature could be very close to the temperature of the

329   porous metal. Therefore, the effect of the mass flow rate fluctuation on the solar

330   receiver outlet temperature is very small.

331   Fig. 9 presents a comparison of the power for the concentrated solar radiation

332   and receiver power. For the case of the nearly constant solar irradiance of 600 W/m^2,

333   the concentrated solar radiation power (E_D) is maintained at around 22.5 kW with the

334   fluctuation lower than $\pm10\%$. In addition, the accurate control system can make sure

335   the reflection focus located at the aperture of the receiver. The red line shown in Fig.

336   9 is the receiver power during the testing period. At the first 10 mins, the solar

337   receiver power (E_R) rise quickly from nearly 0 kW to 12 kW. After that, the value of

338   E_R has the same trend with the mass flow rate according to the time. In other words,

339   the mass flow rate has great influence on the solar receiver power. This can be easily

340   explained by the Eq. (3). As previously mentioned, the mass flow fluctuation has little

341   influence on the value of c_{av}, T_{out} and T_{in}, so the solar receiver power is mainly

342   affected by the mass flow rate especially after the starting stage. The maximum solar

343   receiver power is achieved at about 11:50am with the value of 18.5 kW.

344   Fig. 10(a) shows the time series of the solar receiver efficiency. It is found that

345   when the solar receiver turns into steady state, the efficiency of the solar receiver can

346   be above 55%. The peak value of the efficiency is 87%, and finally, the efficiency is

347   maintained at around 60%. And it is also found that the value of $\eta_{th.R}$ has the same

348   trend with the mass flow rate after the receiver entering into steady stage. In other

349   words, the energy efficiency is positively related with the mass flow rate as shown in

350   Fig. 10(b). The main reason for this phenomenon can be explained by Eq. (10). As

351   described above, the concentrated solar radiation power (E_D) is nearly maintained

352   constant at around 22.5 kW, but the mass flow rate has great influence on the solar

353   receiver power (E_R). Therefore, the ratio of E_R and E_D has the positive

354 relationship with the mass flow rate. This is a very beneficial conclusion. Because in

355 out experiment, the mass flow rate is obviously lower than the real solarised gas

356 turbine system. So the efficiency of the real solarised gas turbine system will be very

357 high. Correspondingly, the usage of the gas will be lower and the investment recovery

358 period could be shorter.

359   Fig. 11 demonstrates the evolution of the heat loss factor (U_L'). At the starting

360 point, U_L' is very high (1.17 kW/K) because of the receiver preheating, and then it

361 drops very quickly within the first 5 mins. When the receiver works at steady state,

362 the heat loss becomes lower and U_L' achieves the minimum value of 0.014 kW/K. In

363 the current study, the heat loss mainly consist of the conduction heat loss, conviction

364 heat loss and radioactive heat loss. Conduction heat loss could be reduced by using

365 material with low thermal conductivity. In the present work, the receiver is

366 surrounded by Aluminum silicate whose thermal conductivity is $0.06 \, \text{W/m}^2 \, \text{K}^{-1}$. The

367 Aluminum silicate can be acted as the thermal insulator to minimize the heat loss.The

368 thermal convection between the solar receiver and ambient is very low as well, this is

369 because the absorbing core is sealed in a pressurized cavity. As a result, only small

370 natural convection occurs around the external cavity of the receiver. It is noted that

371 the use of the insulator could obviously reduce the natural convection. The radioactive

372 heat loss is also an important part of the heat loss, but it can be reduced by using small

373 aperture, as shown in Fig 4. In the design of solar receiver, choosing appropriate

374 aperture diameter is very important for the receiver performance.

375   Fig. 12 shows the comparison between the receiver exergy (Ex_R) and the

376   concentrated solar energy as well as the receiver energy. From this figure, the exergy

377   rate and energy rate vary in a similar manner, the mass flow rate also has the same

378   influence on the exergy rate. It is noted that the highest value of the exergy rate during

379   the test period is around 7.28 kW, whereas the maximum energy rate can reach 18.5

380   kW. It can be concluded that the quality of the energy from the receiver is low due to

381   a large amount of irreversible energy changes such as heat losses and the transfer of

382   high quality solar energy to a fluid that circulating at a relatively low temperature.

383   From Eq. (13), it can be concluded that under the same temperature difference$(T_{out} -$

384     $T_{in})$ and the same energy rate $\dot{m}c_{av}(T_{out} - T_{in})$ condition, increasing the receiver

385   inlet temperature (T_{in}) can achieve higher exergy rate (Ex_R). This will be very

386   helpful for the design of the solar power system. As a result, some recuperator or heat

387   exchanger should be used in the inlet of the solar receiver to recover the waste heat

388   and increase the solar inlet temperature.

389   Fig. 13 presents the comparison between the energy efficiency and exergy

390   efficiency. It is shown from Fig. 13 that similar trends in the exergy efficiency and the

391   energy efficiency are obtained. The highest exergy efficiency is approximately 36%,

392   whereas the highest energy efficiency is around 87%. This suggests that low quality

393   energy obtained from the receiver. It is because the inlet temperature of the receiver is

394   lower than 316 K, whereas the outlet temperature is very high and with the maximum

395   value of 850 K. The temperature ratio (T_{out}/T_{in}) is very high so that too much exergy

396   loss is observed. Therefore, increasing the inlet temperature could be a potential way

397   to increase the exergy efficiency.

398   Fig.14 shows the exergy factor plotted as a function of the temperature

399   difference between the outlet and inlet temperature of the receiver with a linear fitting

400   equation. The exergy factor is also usually used as a measure of the performance of

401   the receiver. Obviously, as the temperature difference increases, the exergy factor also

402   increases. This plot suggests that the higher exergy factor can be obtained when high

403   temperature difference is available. As seen from this figure, the highest exergy factor

404   is 0.41 during the entire test.

405   **5.   Conclusions**

406   This paper performed an experimental study to investigate the thermal

407   performance of a pressurized volumetric solar receiver under real solar radiation

408   condition. The mass flow rate is variable during the experimental process. A parabolic

409   dish with solar tracker system is designed and analysed using energy and exergy

410   analyse method. Experimental results reveal that the solar irradiance is almost stable

411   and maintained at around 600 W/m^2 from 10:00 am to 12:00 pm. It takes about half

412   an hour to rise the solar receiver outlet temperature from 42 $^{\circ}$C to 430 $^{\circ}$C. After 10:30

413   am, the outlet temperature increases very slowly with the time. The mass flow rate

414   fluctuation has little effect on the solar receiver outlet temperature. However, the mass

415   flow rate has great influence on the solar receiver power, energy efficiency and

416   exergy efficiency. The efficiency of the solar receiver can be above 55%. The peak

417 value of the efficiency is 87%, and finally, the efficiency is maintained at around 60%.

418 During the steady state, the heat loss becomes lower and U_L' achieves the minimum

419 value of 0.014 kW/K. The highest exergy efficiency is approximately 36%, whereas

420 the highest energy efficiency is around 87%. As the temperature difference increases,

421 the impact of the exergy factor increases. The highest exergy factor is 0.41 during the

422 entire test.

423

424 **Acknowledgements**

427 **References**

428 [1] Steinfeld A. 2005. Solar thermochemical production of hydrogen - a review.

429   Solar Energy, 78:603-15.

430 [2] Le Roux WG, Bello-Ochende T, Meyer JP. 2011. Operating conditions of an

431   open and direct solar thermal Brayton cycle with optimised cavity receiver and

432   recuperator. Energy, 36:6027-36.

433 [3] Uri Fisher, Chemi Sugarmen, Arik Ring, Joseph Sinai, 2004. Gas Turbine

434   "Solarization"-Modifications for Solar/Fuel Hybrid Operation, J. Sol. Energy

435   Eng. 126(3), 872-878

436 [4] Peter Heller, Markus Pfänder, Thorsten Denk, Felix Tellez, Antonio Valverde,

437   Jesús Fernandez, Arik Ring, 2006. Test and evaluation of a solar powered gas

438   turbine system, Solar Energy, 80(10), 1225-1230

439   [5]   Peter Schwarzbözl, Reiner Buck, Chemi Sugarmen, Arik Ring, Ma Jesús

440   Marcos Crespo, Peter Altwegg, Juan Enrile, 2006. Solar gas turbine systems:

441   Design, cost and perspectives, Solar Energy, 80(10), 1231-1240

442   [6]   Chen Lingen, Zhang Wanlin, Sun Fengrui, 2007. Power efficiency

443   entropy-generation rate and ecological optimization for a class of generalized

444   irreversible universal heatengine cycles. Appl. Energy, 84:512-25.

445   [7]   Matthew Neber, Hohyun Lee, 2012. Design of a high temperature cavity receiver

446   for residential scale concentrated solar power. Energy, 47:481-487

447   [8]   Fernandez P., Miller F. J., 2015. Performance analysis and preliminary design

448   optimization of a small particle heat exchange receiver for solar tower power

449   plants, Solar Energy, 112:458-68.

450   [9]   Fernandez, P., 2013. Numerical-Stochastic Modeling, Simulation and Design

451   Optimization of Samll Particle Solar Receviers for Concentrated Solar Power

452   Plants. Proyecto Fin de Carrera, University of Valladolid, Span.

453   [10] Buck R, Brauning T, Denk T, Pfander M, Schwarzbozl P, Tellez F. 2001.

454   Solar-hybrid gas turbine-based power tower systems, J. Sol. Energy Eng.

455   124(1):2-9.

456   [11] Hischier I., Hess D., Lipinski W., Modest M., Steinfield A., 2009. Heat transfer

457   analysis of a novel pressurized air receiver for concentrated solar power via

458   combined cycles. J. Thermal Sci. Eng. Appl. 1:1-6.

459 [12] Hischier I., Hess D., Lipinski W., Modest M., Steinfield A., 2009. Heat transfer

460   analysis of a novel pressurized air receiver for concentrated solar power via

461   combined cycles. ASME, Vol. 1 / 041002-1.

462 [13] Cui F.Q., He Y.L., Cheng Z.D., Li D., Tao Y.B., 2012, Numerical simulations of

463   the solar transmission process for a pressurized volumetric receiver, Energy,

464   46:618-628

465 [14] Wang M., Siddiqui K., 2010. The impact of geometrical parameters on the

466   thermal performance of a sola receiver of dish-type concentrated solar energy

467   system. Renew. Energy, 35:2501-13.

468 [15] Lu J., Ding J., Yang J., Yang X., 2012. Exergetic optimization for solar heat

469   receiver with heat loss and viscous dissipation, Solar Energy, 86: 2273-81.

470 [16] Song Xingwang, Dong Guobo, Gao Fangyuan, Diao Xungang, Zheng Liqing,

471   Zhou Fuyun, 2014, A numerical study of parabolic trough receiver with

472   no-uniform heat flux and helical screw-tape inserts, Energy, 77:771-782

473 [17] Le Roux W.G., Bello-Ochende T., Meyer J.P., 2011, Operating conditions of an

474   open and direct solar thermal Brayton cycle with optimized cavity receiver and

475   recuperator, Energy, 36:6027-6036

476 [18] Jianfeng Lu, Jing Ding, Jianping Yang, Xiaoxi Yang, 2013, Nonuniform heat

477   transfer model and performance of parabolic trough solar receiver, Energy,

478   59:666-675

479   [19] Flesch R., Stadler H., Uhlig R., 2014. Numerical analysis of the influence of

480   inclination angle and wind on the heat losses of cavity receivers for solar thermal

481   power towers, Solar Energy, 110:427-37.

482   [20] Min Wei, Yilin Fan, Lingai Luo, Gilles Flamant, 2015. Fluid flow distribution

483   optimization for minimizing the peak temperature of a tubular solar receiver,

484   Energy, 91:663-677

485   [21] Tu N., Wei J., Fang J., 2015. Numerical investigation on uniformity of heat flux

486   for semi-gray surfaces inside a solar cavity receiver, Solar Energy, 112:128-43.

487   [22] Capeillere J., Toutant A., Olalde G., Boubault A., 2014. Thermomechanical

488   behavior of a plate ceramic solar receiver irradiated by concentrated sunlight,

489   Solar Energy, 110: 174-87.

490   [23] Wang F., Tan J., Ma L., Shuai Y., Tan H., Leng Y., 2014. Thermal performance

491   analysis of porous medium solar receiver with quartz window to minimize heat

492   flux gradient, Solar Energy, 108: 348-59.

493   [24] Torres Reyes E, Picon Nunez M, Cervantes de GJ. 1998. Exergetic analysis and

494   optimization of a solar-assisted heat pump. Energy, 23(4):337e44.

495   [25] Ameri M., Behbahaninia A., Abbas Tanha A., 2010. Thermodynamic analysis of

496   a tri-generation system based on micro-gas turbine with a steam ejector

497   refrigeration system. Energy, 35:2203-9.

498   [26] Blanco-Marigorta AM, Victoria Sanchez-Henríquez M, Peña-Quintana JA. 2011,

499   Exergetic comparison of two different cooling technologies for the power cycle

500   of a thermal power plant. Energy, 36:1966-72.

501   [27] Sarkar J. 2010. Thermodynamic analyses and optimization of a recompression

502   N_2O Brayton power cycle. Energy, 35:3422-8.

503   [28] Wu C, Chen L, Sun F., 1996, Performance of a regenerative Brayton heat engine.

504   Energy, 21(2):71-6.

505   [29] Jianqin Zhu, Kai Wang, Hongwei Wu, Dunjin Wang, Juan Du, A.G.Olabi,

506   Experimental investigation on the energy and exergy performance of a coiled

507   tube solar receiver, Applied Energy, 2015, 156: 519-527

508   [30] Kai Wang, Hongwei Wu, Dunjin Wang, Yongsheng Wang, Zhiting Tong, Feng

509   Lin, A.G. Olabi, Experimental Study on a Coiled Tube Solar Receiver under

510   Variable Solar Radiation Condition, Solar Energy, 2015,122: 1080–1090

511   [31] Mawire A., Taole S., 2014. Experimental energy and exergy performance of a

512   solar receiver for a domestic parabolic dish concentrator for teaching purposes.

513   Energy Sustain. Dev. 19:162-9.

514   [32] Macphee D., Dincer I., 2009. Thermal modeling of a packed bed thermal energy

515   storage system during charging. Appl. Therm. Eng. 29:695-705.

516   [33] Petela R., 2003. Exergy of undiluted thermal radiation. Solar Energy, 74:469-88.

517   [34] Moffat RJ. Describing the uncertainties in the experimental results. Exp. Therm.

518   Fluid Sci., 1988; 1:3-17

P T   P T

Outlet

Flow meter

Receiver

Boom

Air tank

Dish

Compressor

Inlet   Filter

Pedestal   Control cabinet
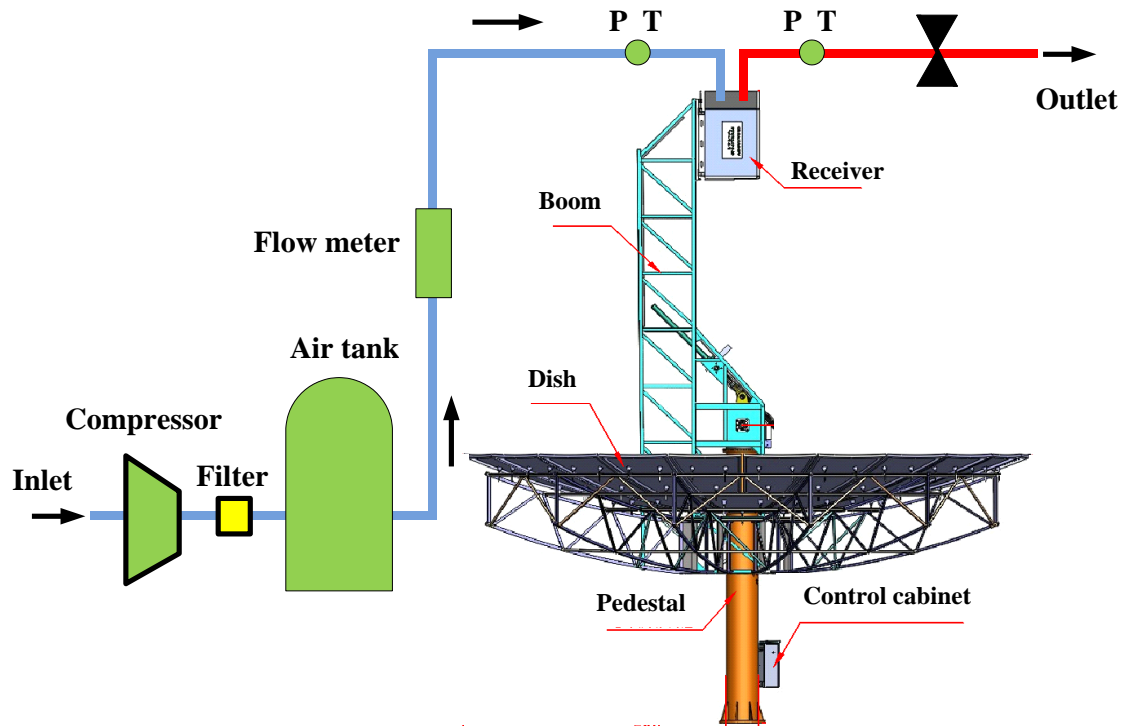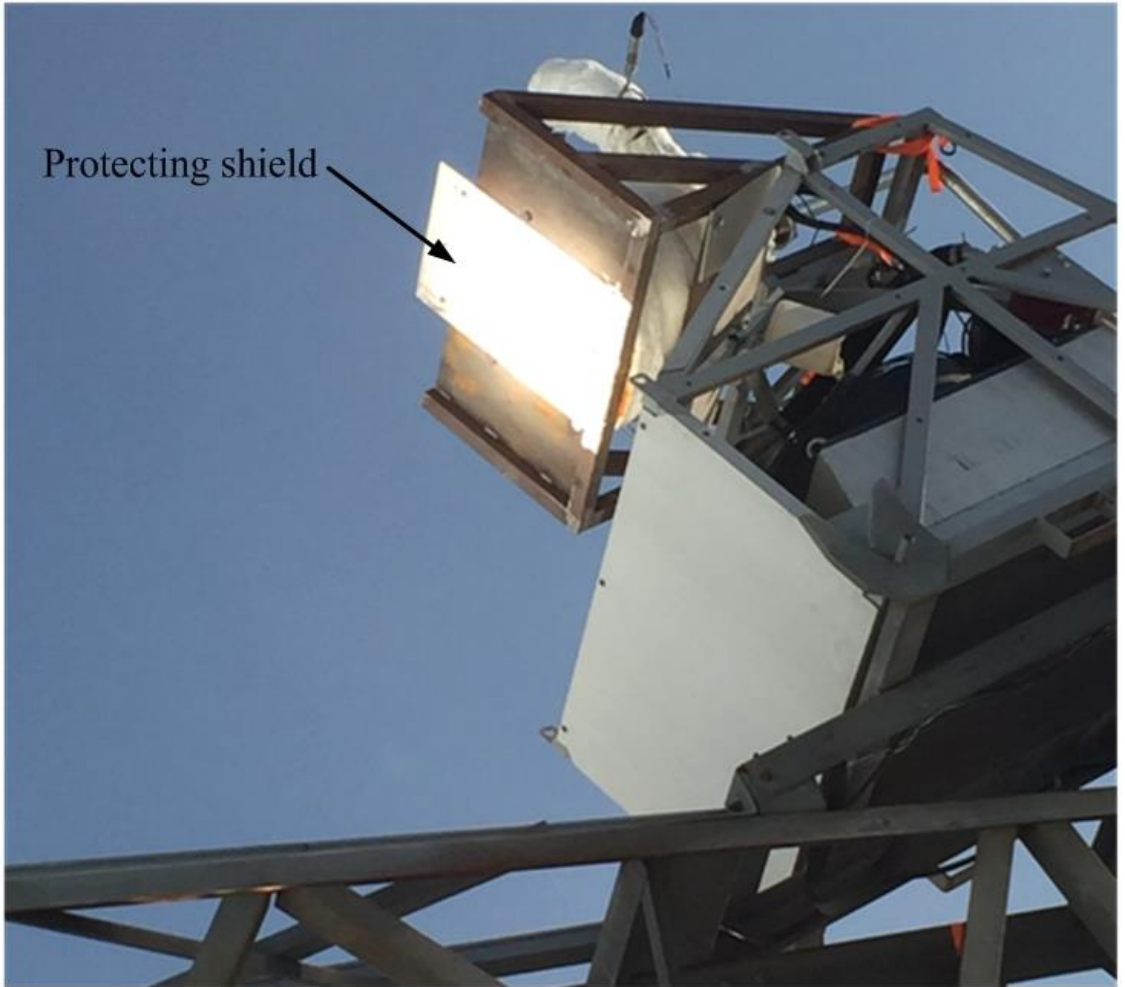
519   [35]

520   [36] **Fig. 1.**   Schematic drawing of experimental test rig.

521 [37]

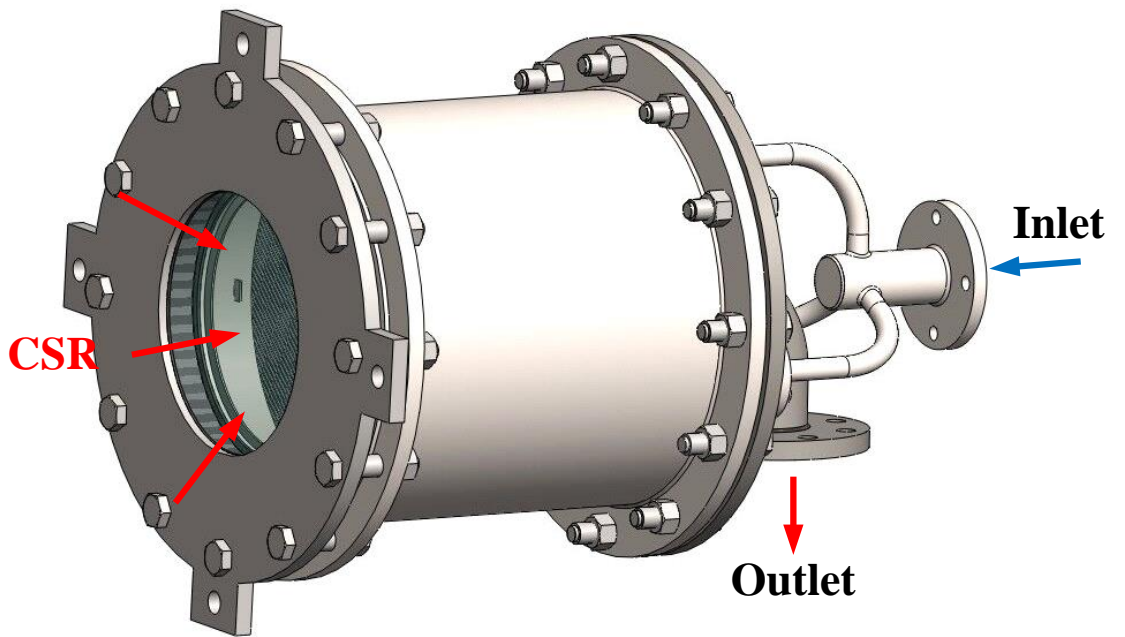522 [38] **Fig. 2.** Parabolic dish.

Protecting shield

523 [39]
524   [40] **Fig. 3.** Protecting shield under the concentrated solar radiation.

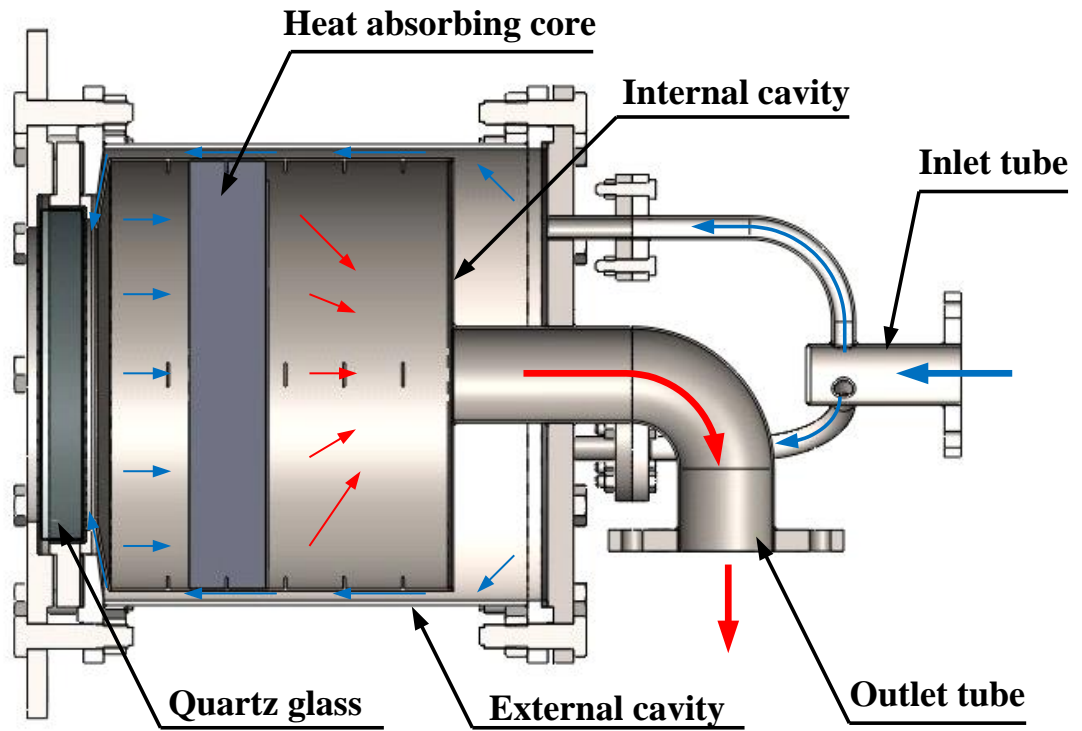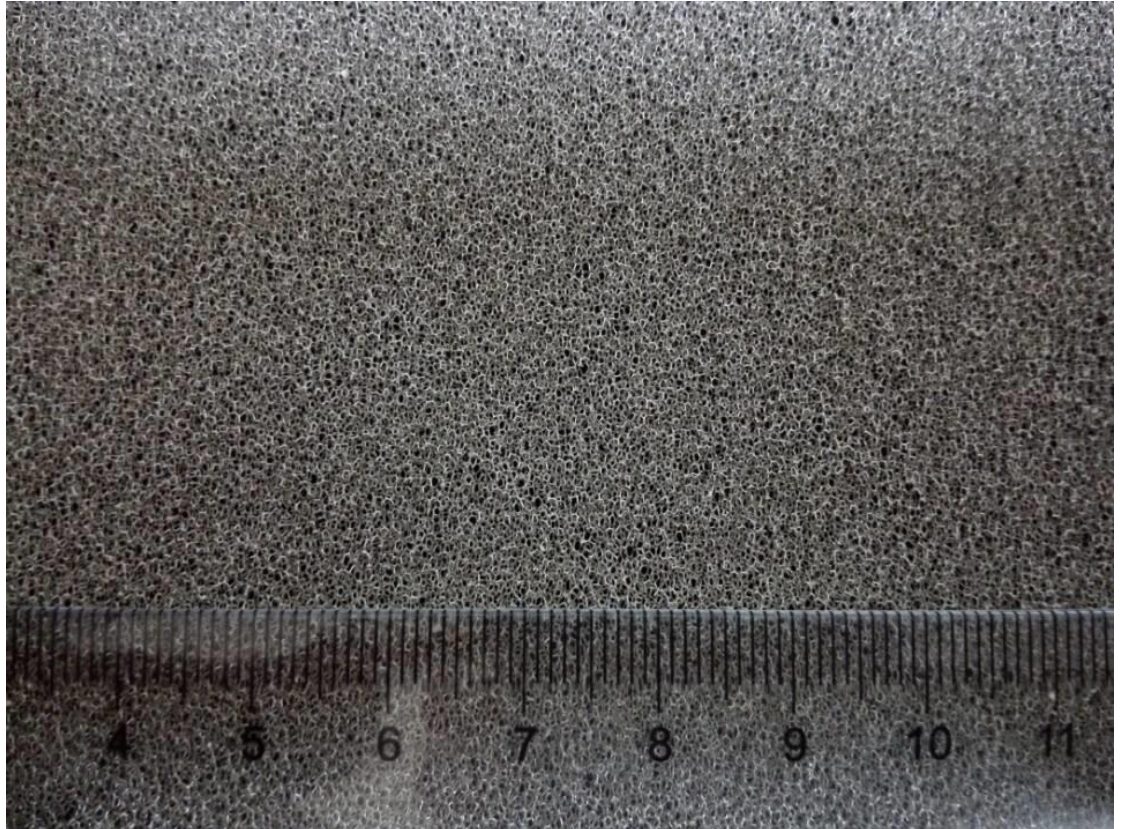

Inlet

CSR

Outlet

525 [41]
526   [42]   **(a)**
527   [43]

Heat absorbing core

Internal cavity

Inlet tube

Outlet tube

Quartz glass

External cavity

528   [44]

529   [45] **(b)**

530   [46] **Fig. 4.** Pressurized volumetric solar receiver. (a) 3D model, (b) cross sectional

531   view.

532   [47]

533   [48] **Fig.5.** Nickel foam.
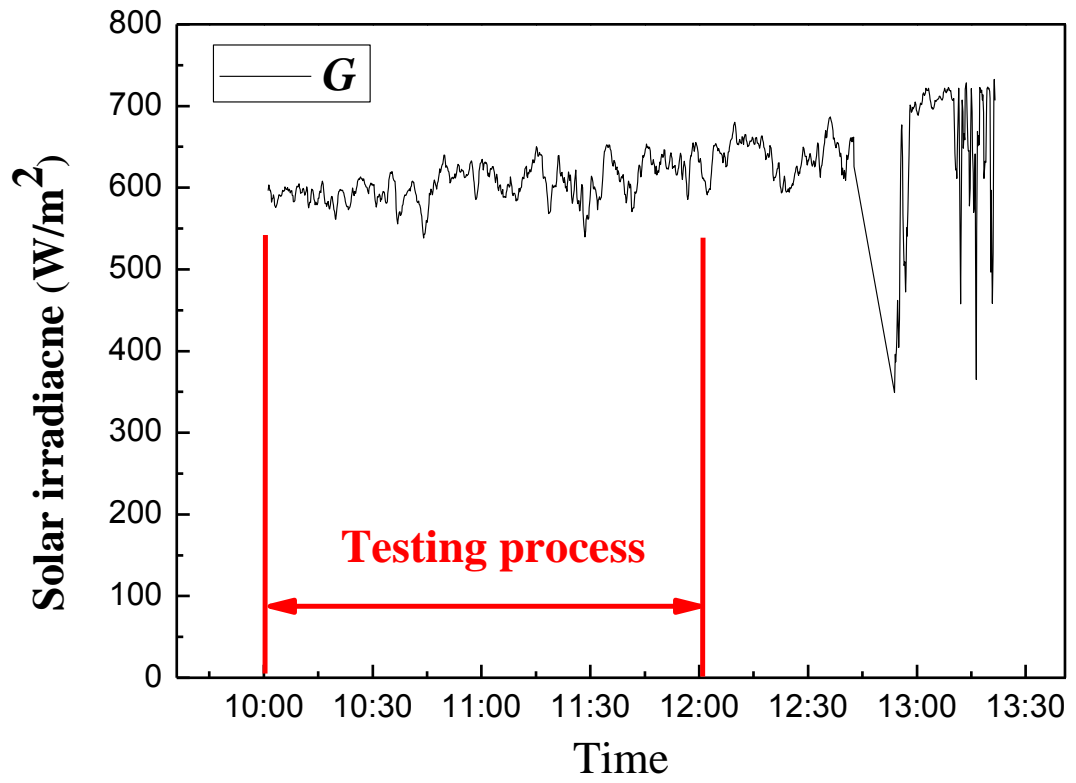
534 [49]

535   [50] **Fig. 6.** Solar irradiance data during the day.
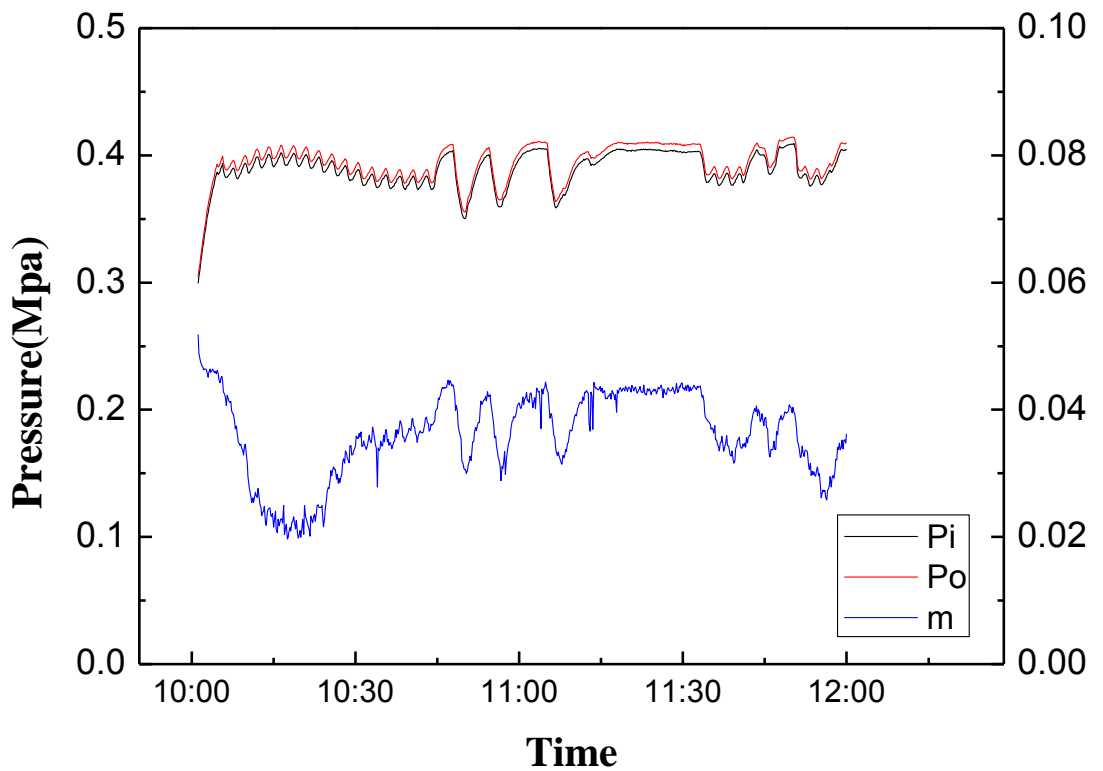
536 [51]

537   [52] **Fig. 7.** Variation of the inlet pressure, outlet pressure and mass flow rate.
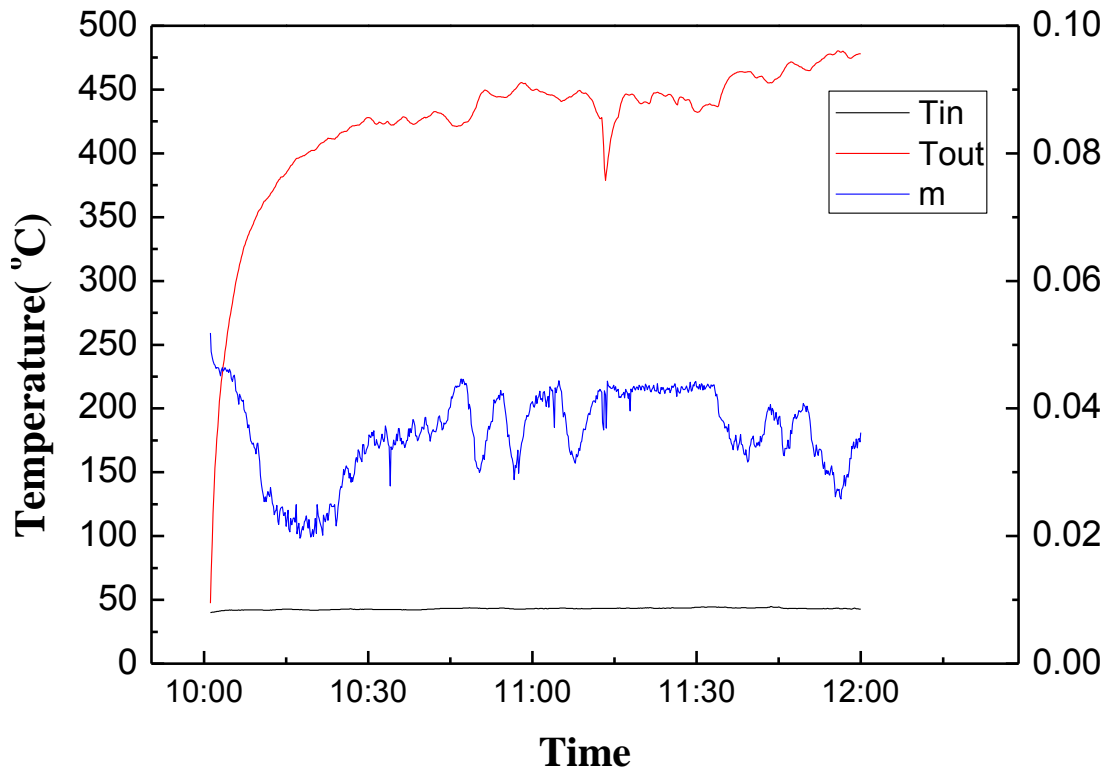
538 [53]
539 [54] **Fig. 8.** Variation of the inlet temperature, outlet temperature and mass flow rate.
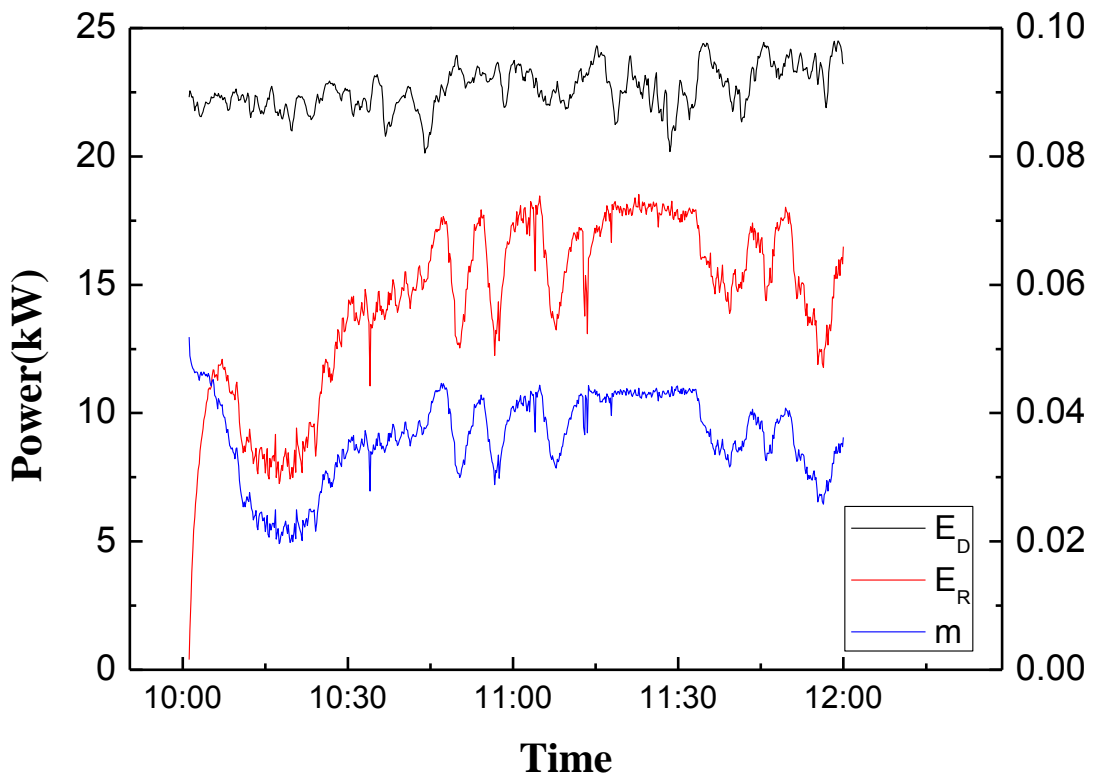
540 [55]
541 [56] **Fig. 9.** Variation of the dish power, receiver power and mass flow rate.
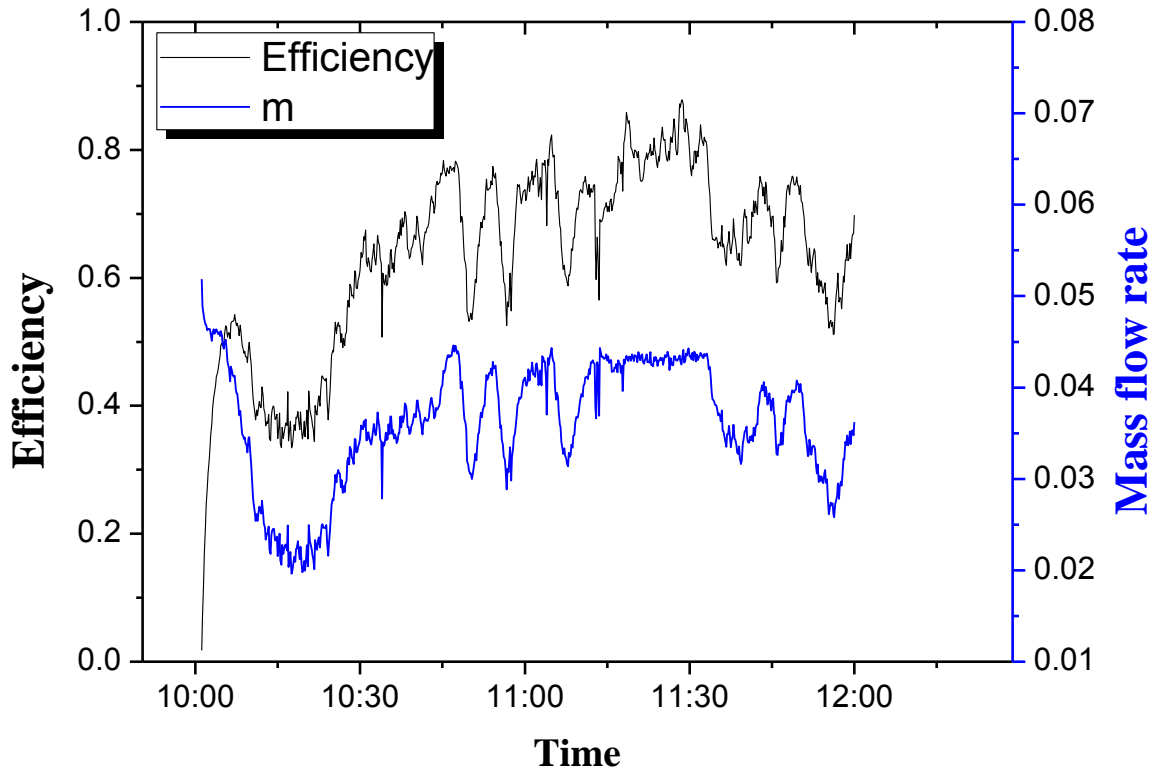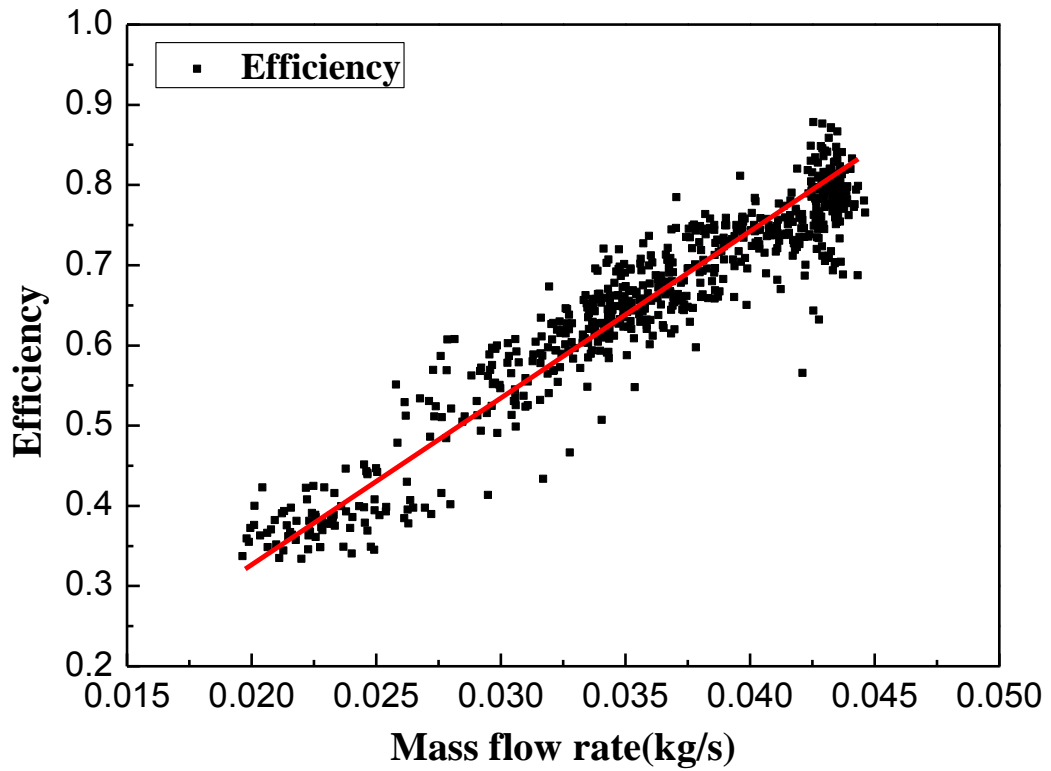
542 [57]
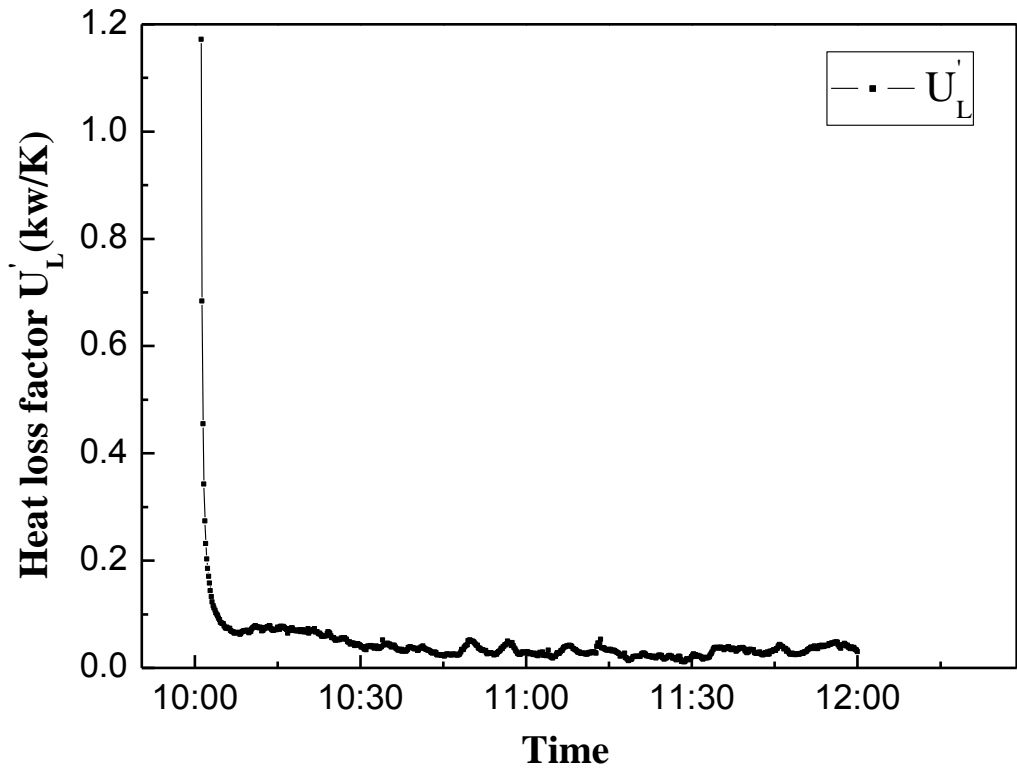543   [58] **(a)**
544   [59]

545 [60]
546   [61] **(b)**
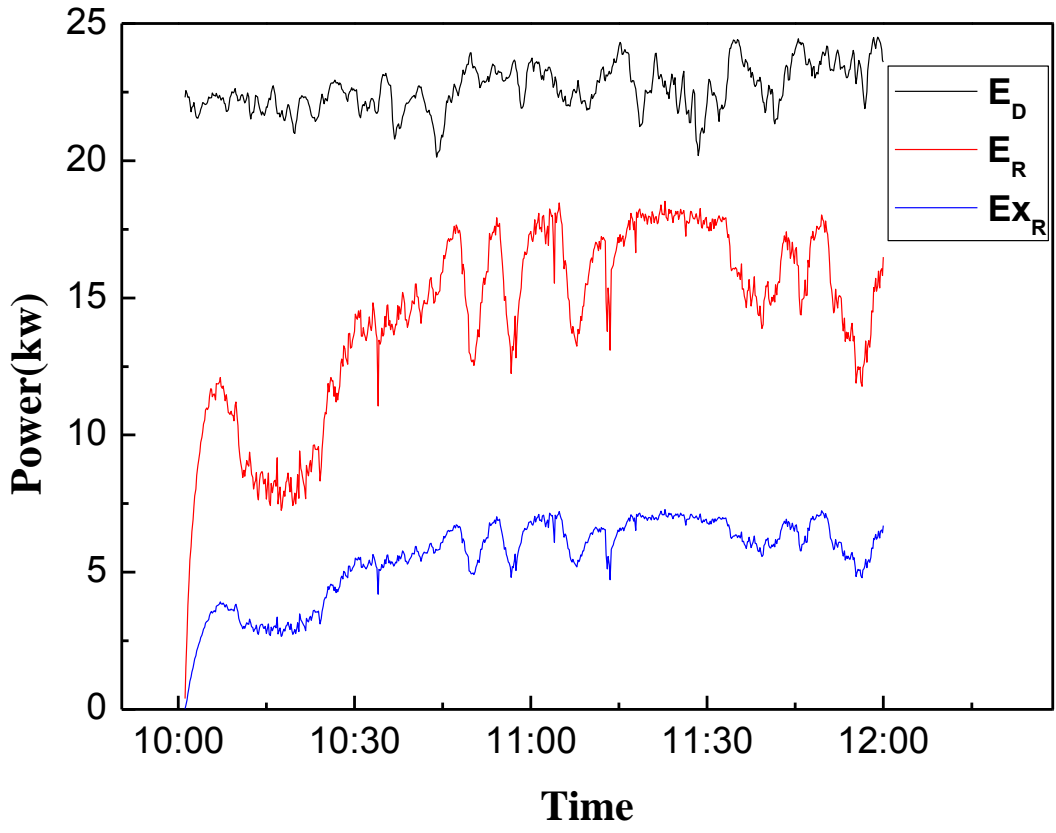547 [62] **Fig. 10.** Efficiency results. (a) during the test period, (b) efficiency vs. mass flow
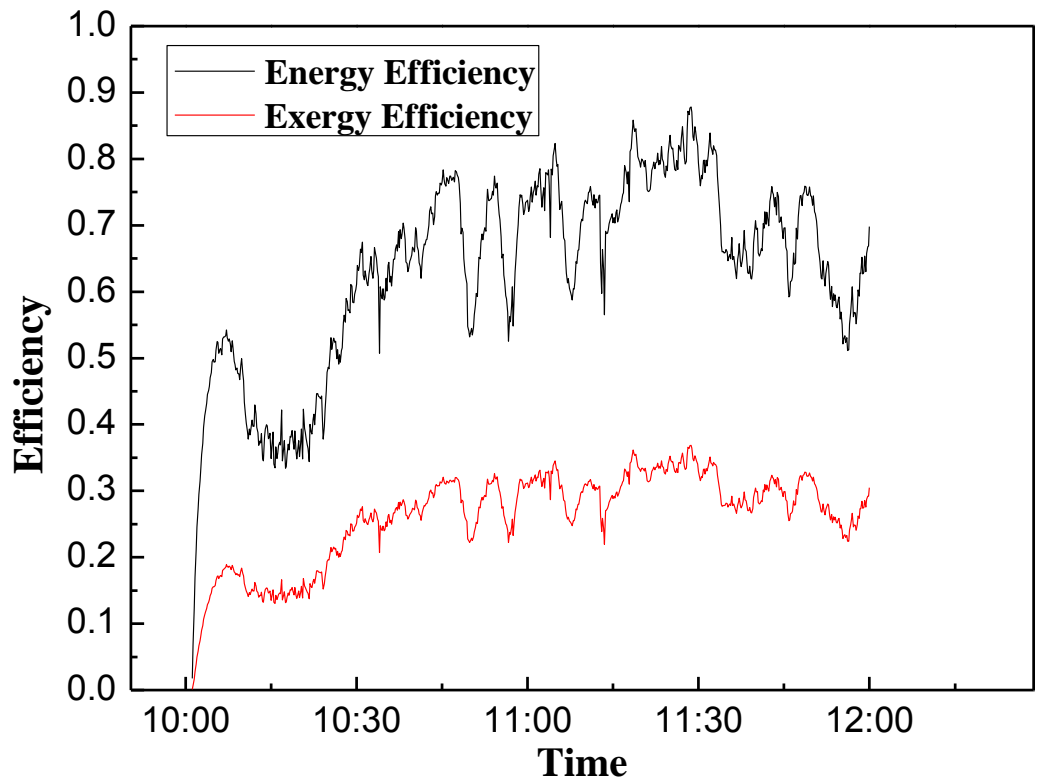548   rate.

549   [63]

550   [64] **Fig. 11.** Heat loss factor profile during the test period.
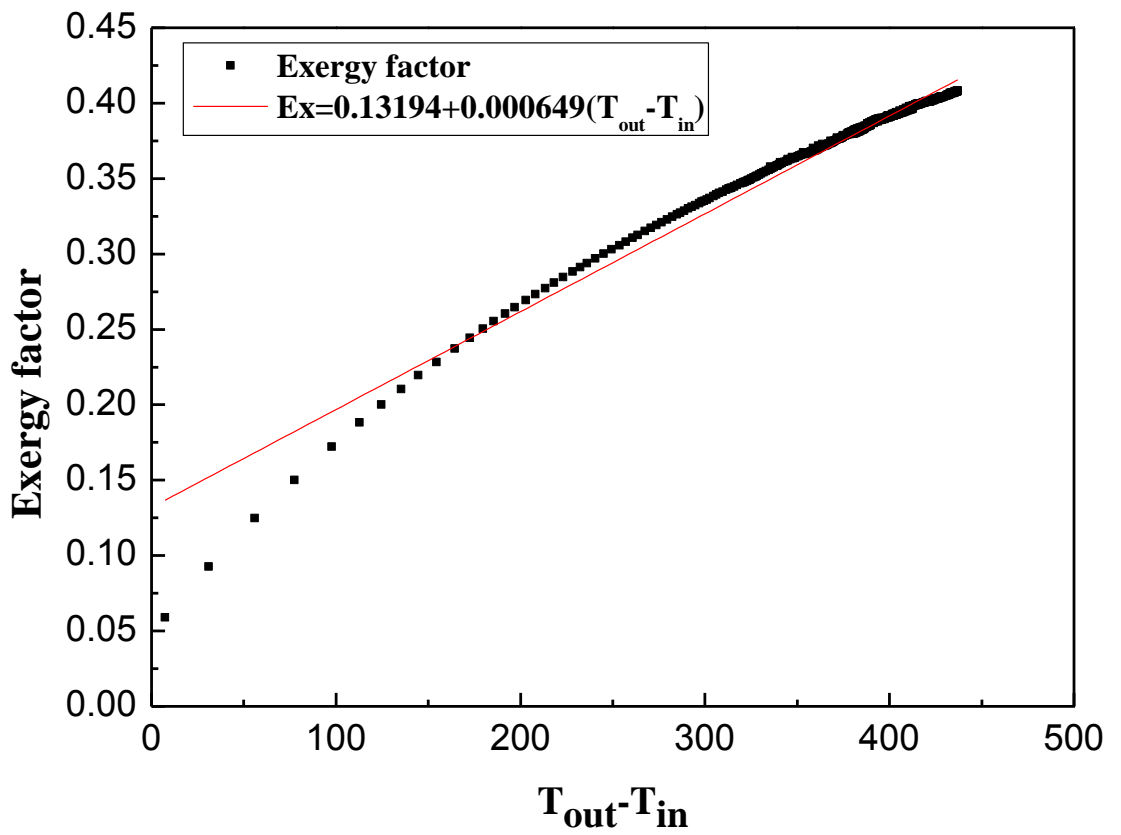

551   [65]

552   [66]   **Fig. 12.** Variation

553   of the power for the receiver energy and exergy

554   [67] during the test period.

555 [68]

556   [69] **Fig. 13.** Energy and Exergy efficiency profile during the test period.

557 [70]

558   [71] **Fig. 14.** The effect of temperature difference on the exergy factor.

559 [72]